A Robust Human-Autonomy Collaboration Framework With Experimental Validation

M. Yusuf Uzun, Emirhan Inanc, and Yildiray Yildiz, *Senior Member, IEEE*

***Abstract*—In this letter, we introduce a robust human-autonomy collaboration framework focusing on flight control applications. The objective is to optimize performance by always keeping the human operator in control of the vehicle while compensating for human limitations. A significant aspect of this framework is its robustness to human intent estimation errors. This is achieved by precisely modulating the automation assistance to prevent undesired interference with the human operator. We provide human-in-the-loop experimental results, demonstrating significant performance improvements when intent estimation is accurate. Experiments also validate that the pilots maintain vehicle control even when the estimation is faulty.**

***Index Terms*—Shared control, adaptive control, human in the loop, long short term memory, uncertain systems.**

I. Introduction

IT'S CRUCIAL that automation systems permit human intervention in critical scenarios, ensuring that the system does not override human decision-making [1]. In shared control systems, there is always a danger of human-machine conflict, and for safety reasons, we want humans to have a higher authority than the machine [2]. To avoid undesired human-machine conflicts, researchers have proposed collaboration schemes based on arbitration mechanisms. These mechanisms adjust the timing and scale of human and automation control inputs, according to the requirements of the system [3], [4], [5].

To develop shared control frameworks, accurately modeling human operators is important for predicting their responses during the design phase. In the context of flight control, the literature offers several control-theory-based pilot models [6]. In our recent work, [7] we introduce the use of an adaptive model to simulate pilot behavior, which shares control with a long short-term memory (LSTM) network. This approach has proven effective in simulations. Inspired by this result, we propose a robust human-autonomy collaboration framework. We use an LSTM network that is trained using an adaptive pilot model [8], to predict and compensate for the errors caused by the operator. A key feature that sets this framework apart from previous findings is its resilience to errors in estimating the intentions of the human operator. This resilience is obtained by modulating the LSTM control input with the degree of correlation between the calculated effects of the pilot input alone and the total control input. Moreover, we analyze the framework with human-in-the-loop experiments. Results demonstrate substantial improvement in tracking performance when the intention estimation is accurate, as well as the system's capability to allow for undisturbed operation by the human operator in the case of faulty intention estimation. This shows the framework's potential for improving performance without compromising operator authority.

The notation $\mathbb{R}^{p\times q}$, $\mathbb{S}^{p\times p}$, $\mathbb{D}^{p\times p}$, and $\mathbb{R}_{+}^{p\times p}$ represents the sets of real, symmetric real, diagonal, and positive definite real matrices, respectively. $\|.\|$ denotes the Euclidean norm for vectors and the induced 2-norm for matrices. The Frobenius norm for matrices is $\|\cdot\|_F$, while Tr{.} is the trace operator. The minimum eigenvalue of a matrix A is expressed as $\lambda_{\min}(A)$. The element-wise projection operator [9], $\text{Proj}(\hat{\theta}(t), Y)$, is used to constrain elements $\hat{\theta}_{i,j}(t)$ of an adaptive parameter $\hat{\theta}(t)$ within a compact set $[\hat{\theta}_{\min_{i,j}}, \hat{\theta}_{\max_{i,j}}]$.

II. Training Setup

To train the LSTM network, it is practical to use models that simulate human behavior, minimizing the need for extensive experiments. The fact that humans can adjust themselves to dynamic environments encourages the use of adaptive models. In this letter, we chose the human model developed by Habboush and Yildiz [8], [10].

The block diagram in Figure 1 describes the designed control architecture for the training, which can be divided into inner and outer loops. In the inner loop, there is an adaptive controller that adjusts the plant's states to follow those of a reference model in the presence of uncertainties, while in the outer loop, a human model and an LSTM network send commands to the inner loop to track a given reference. This LSTM is trained specifically to facilitate the tracking of the human model, which will be explained in Section II-C.

A. Model Reference Adaptive Controller

The plant dynamics are given by

Received 16 September 2024; accepted 18 September 2024. Date of publication 24 September 2024; date of current version 1 October 2024. This work was supported by the Scientific and Technological Research Council of Turkey under Grant 121E384. Recommended by Senior Editor K. Savla. *(Corresponding author: M. Yusuf Uzun.)*

The authors are with the Department of Mechanical Engineering, Bilkent University, 06800 Ankara, Türkiye (e-mail: yusuf.uzun@bilkent.edu.tr; emirhan.inanc@bilkent.edu.tr; yyildiz@bilkent.edu.tr).

Digital Object Identifier 10.1109/LCSYS.2024.3467188

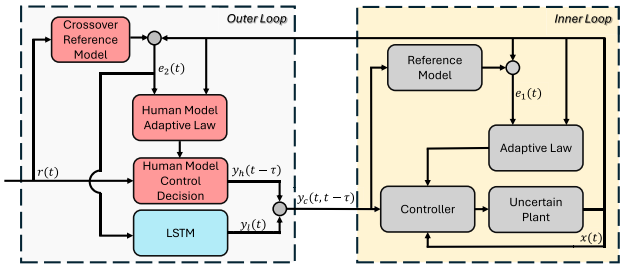

Fig. 1. Block diagram of the overall control architecture used for the training.

$$\dot{x}_p(t) = A_p x_p(t) + B_p \Lambda u_p(t),$$
$$y_1(t) = C_1^T x_p(t), \quad y_2(t) = C_2^T x_p(t), \tag{1}$$

where $x_p(t) \in \mathbb{R}^{n_p}$ is the accessible state vector, $u_p(t) \in \mathbb{R}^m$ is the input vector, $\Lambda \in \mathbb{R}_+^{m\times m} \cap \mathbb{D}^{m\times m}$ is an unknown control effectiveness matrix with the diagonal elements $\lambda_{i,i} \in (0, 1]$, $A_p \in \mathbb{R}^{n_p\times n_p}$ is an unknown system matrix, and $B_p \in \mathbb{R}^{n_p\times m}$ is a known control input matrix, where the pair $(A_p, B_p\Lambda)$ is assumed to be controllable. Moreover, $C_1 \in \mathbb{R}^{n_p\times m}$ and $C_2 \in \mathbb{R}^{n_p\times m}$ are known output matrices, and $y_1(t) \in \mathbb{R}^m$ and $y_2(t) \in \mathbb{R}^m$ correspond to the inner and outer loops.

The inner loop adaptive controller aims to make the plant state $x_p(t)$ track the state $x_r(t) \in \mathbb{R}^{n_p}$ of the reference model,

$$\dot{x}_r(t) = A_r x_r(t) + B_r y_c(t, t-\tau), \ x_r(t_0) = 0. \tag{2}$$

where $A_r \in \mathbb{R}^{n_p\times n_p}$ is Hurwitz, $B_r \in \mathbb{R}^{n_p\times m}$, and $y_c(t, t-\tau) \in \mathbb{R}^m$ is the command to the inner loop, defined by

$$y_c(t, t-\tau) = y_h(t-\tau) + y_l(t), \tag{3}$$

where $y_h \in \mathbb{R}^m$ is the human command with a delay $\tau \in \mathbb{R}^+$, and $y_l \in \mathbb{R}^m$ denotes the command from the LSTM network.

To achieve reference state tracking, nominal dynamics and control input are defined as

$$\dot{x}_n(t) = A_n x_n(t) + B_p u_n(t), \tag{4a}$$
$$u_n(t) = -L_x x_n(t) + L_r y_c(t, t-\tau), \tag{4b}$$

where $L_x \in \mathbb{R}^{m\times n_p}$ is such that $A_r = A_n - B_p L_x$, and $L_r \in \mathbb{R}^{m\times m}$ is selected such that $\lim_{t\to\infty} y_1(t) = y_c$. At the steady state, equation (2) yields $x_r(\infty) = -A_r^{-1} B_p L_r y_c$. This implies that once the reference model's state tracking is achieved, i.e., $\lim_{t\to\infty} x_p(t) = x_r(t)$, the output $y_1(t)$ of the system becomes $y_1(\infty) = -C_1^T A_r^{-1} B_p L_r y_c$ (see (1)). Therefore, feedforward gain is set as

$$L_r = -\left(C_1^T A_r^{-1} B_p\right)^{-1}. \tag{5}$$

Considering (1), we assume that there exist ideal unknown control gains $K_x^* \in \mathbb{R}^{m\times n_p}$ and $K_r^* \in \mathbb{R}^{m\times m}$ such that the matching conditions

$$A_p - B_p \Lambda K_x^* = A_r, \quad B_p \Lambda K_r^* = B_r, \tag{6}$$

are satisfied. Since Λ is diagonal positive definite, there exist $\mathrm{diag}(\lambda^*) = \Lambda^{-1}$ with $K_r^* = \Lambda^{-1} L_r = \mathrm{diag}(\lambda^*) L_r$. Denoting adaptive estimates of ideal values as $\hat{K}_x(t) \in \mathbb{R}^{m\times n_p}$ and $\hat{\lambda}(t) \in \mathbb{R}^m$, plant control law is defined as

$$u_p(t) = -\hat{K}_x(t) x_p(t) + \mathrm{diag}\left(\hat{\lambda}(t)\right) L_r y_c(t, t-\tau). \tag{7}$$

Substituting into (1) results in

$$\dot{x}_p(t) = A_r x_p(t) + B_r y_c(t, t-\tau) + B_p \Lambda \mathrm{diag}\left(\tilde{\lambda}(t)\right) L_r y_c(t, t-\tau) - B_p \Lambda \tilde{K}_x(t) x_p(t), \tag{8}$$

where $\tilde{K}_x(t) \triangleq \hat{K}_x(t) - K_x^*$ and $\tilde{\lambda}(t) \triangleq \hat{\lambda}(t) - \lambda^*$.

Subtracting (2) from (8), using the equality $\Lambda \mathrm{diag}(\tilde{\lambda}(t)) L_r y_c(t, t-\tau) = \mathrm{diag}(L_r y_c(t, t-\tau)) \Lambda \tilde{\lambda}(t)$, and defining the inner-loop tracking error as $e_1(t) \triangleq x_p(t) - x_r(t)$, error dynamics can be obtained as

$$\dot{e}_1(t) = A_r e_1(t) + B_p \mathrm{diag}(L_r y_c(t, t-\tau)) \Lambda \tilde{\lambda}(t) - B_p \Lambda \tilde{K}_x(t) x_p(t). \tag{9}$$

Then, adaptive laws for the inner loop are selected as

$$\dot{\hat{K}}_x^T(t) = \gamma_x x_p(t) e_1(t)^T P_1 B_p, \tag{10a}$$
$$\dot{\hat{\lambda}}(t) = \gamma_\lambda \mathrm{Proj}\left(\hat{\lambda}(t), \ -\mathrm{diag}(L_r y_c(t, t-\tau)) B_p^T P_1 e_1(t)\right), \tag{10b}$$

where projection operator, Proj(., .) [9], sets positive bounds on each $\hat{\lambda}_i(t)$, i.e., $\hat{\lambda}_{max_i} > \hat{\lambda}_{min_i} > 0$ for all $i = 1, \ldots, m$. Moreover, $\gamma_x, \gamma_\lambda \in \mathbb{R}_+$ are learning rates, and $P_1 \in \mathbb{R}_+^{n_p\times n_p} \cap \mathbb{S}^{n_p\times n_p}$ is the solution of the Lyapunov equation

$$A_r^T P_1 + P_1 A_r = -Q_1, \tag{11}$$

for some $Q_1 \in \mathbb{R}_+^{n_p\times n_p} \cap \mathbb{S}^{n_p\times n_p}$.

Lemma 1: For the system (1), along with the reference model (2), and the adaptive controller in (7) and (10), the solution $(e_1(t), \tilde{K}_x(t), \tilde{\lambda}(t))$ is Lyapunov stable in the large. Furthermore, $\lim_{t\to\infty} e_1(t) = 0$, and $\dot{\hat{K}}_x(t)$ and $\dot{\hat{\lambda}}(t)$ remain bounded, along with all signals within the inner-loop.

Proof: The command, $y_c(t)$ in (3), is bounded since y_h is bounded due to the limits of the manipulator, and y_l is bounded since LSTM is trained offline, therefore weights do not change during testing, and activation functions are bounded. Therefore, the proof follows from Lemma 1 of [11].

B. Human Model

Outer Loop consists of the human pilot model proposed in [8], and the LSTM network. The human operator controls the system such that the plant states follow those of a unity feedback reference model, referred to as the *crossover-reference model* (Figure 1), given as

$$\dot{x}_m(t) = A_m x_m(t) + B_m r(t-\tau), \tag{12}$$

where $x_m(t) \in \mathbb{R}^{n_p}$ is the reference model state vector, $r(t) \in \mathbb{R}^m$ is a bounded reference input, $A_m \in \mathbb{R}^{n_p\times n_p}$ is Hurwitz and $B_m \triangleq B_r \theta_r \in \mathbb{R}^{n_p\times m}$. Similar to the selection of L_r in (5), the nominal feed-forward gain $\theta_r \in \mathbb{R}^{m\times m}$ is selected as

$$\theta_r = -\left(C_2^T A_m^{-1} B_r\right)^{-1}, \tag{13}$$

to achieve $\lim_{t\to\infty} y_2(t) = r$ if $\lim_{t\to\infty} x_p(t) = x_m(t)$. It is also assumed that there exists $\theta_x \in \mathbb{R}^{m\times n_p}$ such that $A_m = A_r - B_p L_r \theta_x$ The human control input is given in [8] as

$$\mathcal{G}(t) = \hat{\Phi}_1(t)x_p(t) + \theta_r r(t) + \int_{-\tau}^{0} \hat{\Phi}_2(t,\eta)L_r y_h(t+\eta)\,\mathrm{d}\eta, \tag{14a}$$

$$v(t) = L_r^{-1}\mathrm{diag}\Big(\hat{\lambda}_2(t)\Big)L_r\mathcal{G}(t), \tag{14b}$$

$$y_{h_i}(t) = \begin{cases} v_i(t), & \text{if } |v_i(t)| \le y_{o_i}, \\ y_{o_i}\mathrm{sgn}(v_i(t)), & \text{if } |v_i(t)| > y_{o_i}, \end{cases} \tag{14c}$$

where $\hat{\Phi}_1(t) \in \mathbb{R}^{m\times n_p}$, $\hat{\Phi}_2(t,\eta) \in \mathbb{R}^{m\times m}$ and $\hat{\lambda}_2(t) \in \mathbb{R}^m$ are the adaptive estimations of the ideal values

$$\begin{aligned} \Phi_1^*(t) &= \bar{H}(t)\Phi(t+\tau,t), \\ \Phi_2^*(t,\eta) &= \bar{H}(t)\Phi(t+\tau,t+\eta+\tau)B_p\Lambda_2(t+\eta+\tau), \end{aligned} \tag{15}$$

and $\lambda_2^*(t)$, respectively, where $\bar{H}(t) \triangleq -(\theta_x + L_r^{-1}H^T(t+\tau))$, $H^T(t) \triangleq -\Lambda\tilde{K}_x(t)$, and $\Lambda_2(t) \triangleq \Lambda\mathrm{diag}(\hat{\lambda}(t))$. Since the projection operator in (10b) enforces positive lower bounds on $\hat{\lambda}(t)$, $\Lambda_2(t) \in \mathbb{D}_+$, and $\mathrm{diag}(\lambda_2^*(t)) = \Lambda_2^{-1}(t+\tau)$ exists for all $t \ge 0$. Furthermore, (14c) is an element-wise saturation function where $y_{o_i} \in \mathbb{R}_+$ is the saturation limit of $y_{h_i}(t)$ (the i^{th} element of $y_h(t)$).

The outer-loop error dynamics is derived for the overall system and given as

$$\begin{aligned} \dot{e}_2(t) = {} & A_m e_2(t) + B_p\Lambda_2(t)L_r y_l(t) + B_p\Lambda_2(t)L_r\Delta y(t-\tau) \\ & + B_p\mathrm{diag}(L_r\mathcal{G}(t-\tau))\Lambda_2(t)\tilde{\lambda}_2(t-\tau) \\ & + B_p L_r\tilde{\Phi}_1(t-\tau)x_p(t-\tau) \\ & + B_p L_r\int_{-\tau}^{0}\tilde{\Phi}_2(t-\tau,\eta)L_r y_h(t+\eta-\tau)\mathrm{d}\eta, \end{aligned} \tag{16}$$

where $e_2(t) \triangleq x_p(t) - x_m(t)$ is the outer-loop tracking error, $\tilde{\Phi}_1(t) \triangleq \hat{\Phi}_1(t) - \Phi_1^*(t)$, $\tilde{\Phi}_2(t,\eta) \triangleq \hat{\Phi}_2(t,\eta) - \Phi_2^*(t,\eta)$ and $\tilde{\lambda}_2(t) \triangleq \hat{\lambda}_2(t) - \lambda_2^*(t)$ are the adaptive parameter estimation errors for the outer-loop, and $\Delta y(t) \triangleq y_h(t) - v(t)$ denotes the control deficiency caused by human input saturation.

An auxiliary signal $e_\Delta(t)$ for human input constraints is generated as in [8] as

$$\dot{e}_\Delta(t) = A_m e_\Delta(t) + B_p\mathrm{diag}\Big(\hat{\lambda}_3(t)\Big)L_r\Delta y(t-\tau),\ e_\Delta(t_0) = 0, \tag{17}$$

where $\mathrm{diag}(\lambda_3^*(t)) = \Lambda_2(t)$, and $\hat{\lambda}_3(t) \in \mathbb{R}^m$ is an adaptive parameter estimate of the ideal value $\lambda_3^*(t)$. Then, the augmented error signal is derived as $e_y(t) \triangleq e_2(t) - e_\Delta(t)$, and the parameters are updated using the following adaptive laws

$$\dot{\hat{\lambda}}_2(t) = \gamma_2\mathrm{Proj}\Big(\hat{\lambda}_2(t),\ -\mathrm{diag}(L_r\mathcal{G}(t-\tau))B_p^T P_2 e_y(t)\Big), \tag{18a}$$

$$\dot{\hat{\lambda}}_3(t) = \gamma_3\mathrm{Proj}\Big(\hat{\lambda}_3(t),\ \mathrm{diag}(L_r\Delta y(t-\tau))B_p^T P_2 e_y(t)\Big), \tag{18b}$$

$$\dot{\hat{\Phi}}_1^T(t) = \gamma_{\phi_1}\mathrm{Proj}\Big(\hat{\Phi}_1^T(t),\ -x_p(t-\tau)e_y^T(t)P_2B_pL_r\Big), \tag{18c}$$

$$\dot{\hat{\Phi}}_2^T(t,\eta) = \gamma_{\phi_2}\mathrm{Proj}\Big(\hat{\Phi}_2^T(t,\eta),\ -L_r y_h(t+\eta-\tau)e_y^T(t)P_2B_pL_r\Big), \tag{18d}$$

where the learning rates are $\gamma_2, \gamma_3, \gamma_{\phi_1}, \gamma_{\phi_2} \in \mathbb{R}_+$, and the solution of the Lyapunov equation $A_m^T P_2 + P_2 A_m = -Q_2$, for some $Q_2 \in \mathbb{R}_+^{n_p\times n_p} \cap \mathbb{S}^{n_p\times n_p}$ is $P_2 \in \mathbb{R}_+^{n_p\times n_p} \cap \mathbb{S}^{n_p\times n_p}$.

While the adaptive human model controlling an adaptive system was developed, and a stability analysis was performed in [8], this letter requires a stability analysis of the entire system with the integrated LSTM network. We first give Lemma 2, which follows the analysis in [8], and then provide the main theorem here. To maintain the focus on the primary contribution, we defer the Theorem proof to the Appendix.

Lemma 2: There exist $\phi \in \mathbb{R}_+$and $\dot{\phi} \in \mathbb{R}_+$ such that

$$\|\Phi(t+\tau,t)\|_F \le \phi,\ \text{for all } t \ge t_0, \tag{19a}$$

$$\|\Phi(t+\tau,t+\eta+\tau)\|_F \le \phi,\ \text{for all } t \ge t_0, -\tau \le \eta \le 0 \tag{19b}$$

$$\|\dot{\Phi}(t+\tau,t)\|_F \le \dot{\phi},\ \text{for all } t \ge t_0, \tag{19c}$$

$$\|\dot{\Phi}(t+\tau,t+\eta+\tau)\|_F \le \dot{\phi},\ \text{for all } t \ge t_0, -\tau \le \eta \le 0. \tag{19d}$$

Proof Summary (A Detailed Proof can be Found in [10]): Considering the homogeneous part (HP) of (2), we obtain that $x_r(t) = 0$, and $x_p(t) = e_1(t) + x_r(t) = e_1(t)$ for all $t > t_0$. Then, the origin $x_p(t) = 0$ of the HP of the outer loop dynamics is uniformly stable (Lemma 1). The state transition matrix for the HP of the outer loop dynamics can then be bounded as given in (19a), (19b). Moreover, $\Phi(t+\tau,t)$ can be written as $\Phi(t+\tau,t) = X(t+\tau)X(t)^{-1}$, where X is a *fundamental matrix* [12], and $\dot{X}(t) = A(t)X(t)$ with $A(t) \triangleq (A_r + B_p H^T(t))$. Then, $\dot{\Phi}(t+\tau,t) = A(t+\tau)\Phi(t+\tau,t) - \Phi(t+\tau,t)A(t)$. Since $H^T(t) \triangleq -\Lambda\tilde{K}_x(t)$ is bounded (Lemma 1), $A(t)$ is bounded and there exist $\dot{\phi} \in \mathbb{R}_+$ that satisfies (19c), (19d). ■

Theorem 1: Consider the dynamical system (1), the adaptive controller (2), (7) and (10), and the adaptive human pilot model (12), (14) and (18). Then, there exists $\tau^* \in \mathbb{R}_+$ such that for all $\tau \in [0,\tau^*]$ the solution $(e_y(t), \tilde{\lambda}_2(t), \tilde{\lambda}_3(t), \tilde{\Phi}_1(t), \tilde{\Phi}_2(t,\eta))$ remains bounded for all $t \ge t_0$ and converges to a compact set, and all signals are bounded.

Proof: The proof is given in the Appendix.

C. LSTM Network

We design an LSTM network [13] to help the pilot minimize the reference model tracking error (16). To achieve this, we aim to give reference model tracking error $e_2(t)$ in (16) as input to the LSTM network. However, in experiments where the human operator controls the system, $e_2(t)$ is not available to the LSTM network as an input. Therefore, reference signal is obtained from a predetermined mission, such as a visually determined target from visual sensors, denoted as $r_l(t)$ in Figure 2, and given to the reference model to calculate the estimation of human intention, $x_{m,l}(t) = A_m x_{m,l}(t) + B_m r_l(t-\tau)$. Then, $e_{2,l}(t) \triangleq x_p(t) - x_{m,l}(t)$ is given to the LSTM network as an input, which in turn computes the raw LSTM output, denoted as $y_l'(t)$.

The optimal result for the LSTM network is designed to neutralize the elements that lead to errors in tracking the reference model. Specifically,

$$\begin{aligned} y_l'(t) = {} & -\Delta y(t-\tau) - L_r^{-1}\Lambda_2^{-1}(t)L_r\tilde{\Phi}_1(t-\tau)x_p(t-\tau) \\ & - L_r^{-1}\Lambda_2^{-1}(t)\mathrm{diag}(L_r\mathcal{G}(t-\tau))\Lambda_2(t)\tilde{\lambda}_2(t-\tau) \\ & - L_r^{-1}\Lambda_2^{-1}(t)L_r\int_{-\tau}^{0}\tilde{\Phi}_2(t-\tau,\eta)L_r y_h(t+\eta-\tau)\mathrm{d}\eta, \end{aligned} \tag{20}$$

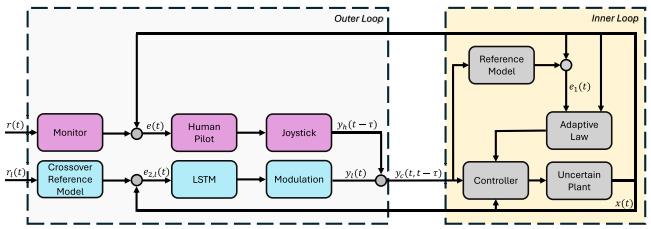

Fig. 2. Block diagram of the overall control architecture used in the experiments.

will lead to the error dynamics being represented as $\dot{e}_2(t) = A_m e_2(t)$. Consequently, this function is chosen as the *truth* (the function that needs to be approximated) for the LSTM to achieve the desired error dynamics.

D. Modulation of LSTM

The LSTM network's input is $e_{2,l}(t)$, an estimation of $e_2(t)$, which can be faulty due to various reasons. Sensors may incorrectly determine the target location, $r_l(t)$ estimation may be erroneous, or the pilot may decide to deviate from a predetermined mission. The LSTM network, receiving a faulty estimation, may hinder pilot control efforts in such cases since LSTM's and the pilot's intentions differ. To detect these cases, we analyze the correlation between the inner loop reference model responses to the pilot input only and to a combination of the pilot and the LSTM inputs. These responses can be calculated as $\dot{x}_{r,h}(t) = A_r x_{r,h}(t) + B_r y_h(t-\tau)$, $y_{2,h} = C_2^T x_{r,h}(t)$, for the pilot input only, and $\dot{x}_{r,l}(t) = A_r x_{r,l}(t) + B_r(y_l'(t) + y_h(t-\tau))$, $y_{2,l} = C_2^T x_{r,l}(t)$, for the pilot and LSTM inputs. We propose that when the correlation between the outputs that are intended to be tracked, $y_{2,h}$ and $y_{2,l}$, decreases, the LSTM's effect should also decrease by scaling the LSTM signal $y_l'(t)$ with a modulation coefficient, ρ_m, such that LSTM input given to the system becomes $y_l(t) = \rho_m y_l'(t)$. This modulation mechanism is based on the following shared control principles: (a) The human operator should be able to regain control authority whenever necessary, (b) LSTM network's actions should remain predictable by the human operator. If the LSTM network's and the human operator's estimations of uncertainties have a considerable difference despite using the same data, the LSTM's influence should be reduced, and (c) if human intention estimation has a large enough error, or the reference tracked by the human operator changes LSTM's effect on the system should diminish.

Modulation coefficient ρ_m is determined by first calculating the Pearson correlation coefficient between $y_{2,h}$ and $y_{2,l}$ as

$$\rho(t_k) = \frac{\sum_{i=k-n}^{k}\big(y_{2,h}(t_i) - \bar{y}_{2,h}\big)\big(y_{2,l}(t_i) - \bar{y}_{2,l}\big)}{\sqrt{\sum_{i=k-n}^{k}\big(y_{2,h}(t_i) - \bar{y}_{2,h}\big)^2}\sqrt{\sum_{i=k-n}^{k}\big(y_{2,l}(t_i) - \bar{y}_{2,l}\big)^2}}, \quad (21)$$

where the bar notation denotes the mean value, t_k refers to a sampling instant, and n is the number of samples within τ_p seconds. Then, the coefficient is calculated as $\rho_m = \exp(-(\rho-1)^2/(0.1^2))$, which can take values between 1 and 0. Based on operator feedback, τ_p is determined as 10 seconds.

III. Experiments

A flight control task is conducted in the configuration given in Figure 2. 16 participants from Bilkent University Mechanical Engineering Department attended the study, which is approved by the Bilkent University Ethics Committee, and informed consent is taken from each subject. The participants monitor the pitch angle of the aircraft and a reference signal through a display. Then, they give pitch rate commands to the inner loop through a Logitech Extreme 3D Pro joystick, where the saturation limits are adjusted to $y_{o_i} = 10$ deg/s for $i = 1, \ldots, 3$ (see (14c)).

A. Inner Loop Parameters

For the plant in (1), a linearized model of a Boeing 747 cruising in level flight at 774ft/sec and an altitude of 40kft is used [10]. States of the plant are velocity along x and z axes, pitch rate, and pitch angle. The control input $u_p(t)$ is the elevator deflection, where magnitude and rate saturation limits are set as $+17/-23$ (deg) and $+37/-37$ (deg/s) [14].

For the inner loop controller, the feedback gain L_x in (4b) is set with LQR cost matrices of $Q_{LQR} = \text{diag}([0.001, 0.01, 10, 0.1])$, and $R_{LQR} = 10$. The Lyapunov matrix in (11) is selected as $Q_1 = 10^{-3} I_{4\times4}$, the learning rates in (10) are set to $\gamma_x = 2$, and $\gamma_\lambda = 4$. Due to a zero at the origin in the transfer function $x_{p3}(s)/u_p(s)$, the inner-loop feed-forward controller is based on the short-period dynamics [15]. Then, L_r is set as $L_r = -(C_{sp}^T A_{sp}^{-1} B_{sp})^{-1}$, where A_{sp}, B_{sp}, and C_{sp} correspond to short-period dynamics.

B. Network Training

LSTM network is trained with simulations using the human model in Section II-B. The parameters of the pilot model are determined using participant data and nonlinear optimization algorithms available in MATLAB. As a result, θ_x is set to $\theta_x = [0.0115, 0.0009, -0.3535, 0.7673]$ and human delay is determined as $\tau = 0.18$ s. θ_r is assigned as shown in (13). The Lyapunov matrix of the human model is taken as $Q_2 = 10^{-3} I_{4\times4}$. The implementation of the finite integral term in (14a) and the adaptive law in (18d) involves discretizing the integral, as demonstrated in [16]. Learning rates are selected as $\gamma_2 = 1.2$, $\gamma_3 = 1.3$, $\gamma_{\phi_1} = 0.8 I_{4\times4}$ and $\gamma_{\phi_2} = 2.2$.

The LSTM network is configured with a single hidden layer of 64 neurons. The input layer has 4 neurons to align with the four states of the outer loop error dynamics. Given that there's a single actuator, the network features one neuron in its fully connected output layer. The LSTM network's weights are initialized using the Xavier method, and Adam optimizer is used for the training. The simulation operates at a step time of 0.01s. The training is completed within 1500 iterations.

During training, we introduce plant and actuator uncertainties (see (1)) such that $A_p = A_n$ and $\Lambda = 1$ for $t \leq 20$, whereas $A_p = A_n - B_p W_{unc}$ and $\Lambda = \Lambda_v$ for $t > 20$, where the elements of the unknown matrix $W_{unc} \in \mathbb{R}^{n_p \times m}$ are randomized by assigning values between -0.2 and 0.2, for each training episode. Similarly, $\Lambda_v \in {\mathbb{R}_+}^{m\times m}$ values are randomly set between 0.5 and 1.

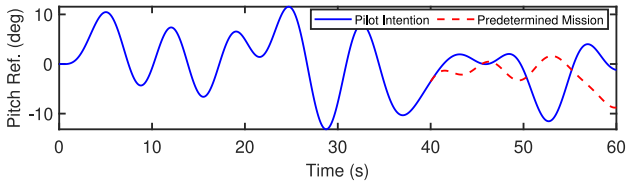

Fig. 3. Pitch references displayed during experiments.

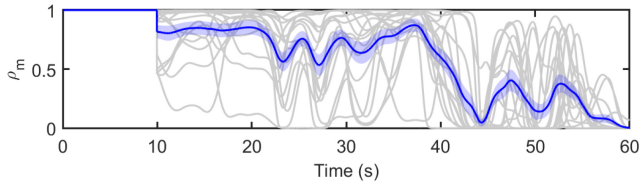

Fig. 4. Evolution of the modulation coefficient across multiple experiments. Gray lines illustrate the individual trajectories, and the blue line represents the mean values with the standard error of the mean.

TABLE I
WORKLOAD (W), PRECISION (P), AND TPX FOR PITCH ANGLE (θ) TRACKING FOR PILOT ONLY AND LSTM AIDED CASES, BY INTERVALS

Interval	Case	W	P	TPX
$0 \leq t < 20$	Pilot Only	1.03	79.39	0.33
	with LSTM	1.05	93.81	0.44
$20 \leq t < 40$	Pilot Only	1.14	58.16	0.20
	with LSTM	1.02	72.85	0.30
$40 \leq t < 60$	Pilot Only	1.14	77.40	0.32
	with LSTM	1.08	74.06	0.30

C. Results

During the experiments, for the first 20 seconds, the pilot tracks the reference without any uncertainty. After 20 seconds, plant and control effectiveness uncertainties are introduced to the system, where A_p in (1) is set to $A_p = A_n - B_p[0.16, 0.10, 0.07, -0.07]$, and the control effectiveness is set to $\Lambda = 0.8$. Lastly, after 40 seconds, the reference signal is separated into two in a continuous manner, as seen in Figure 3. Participants are asked to follow the target labeled as pilot intention, whereas the LSTM network perceives the predetermined mission (following $r_l(t)$) as in Figure 2.

The system is evaluated for two cases, one with the pilot assisted by the LSTM network, and the other with only the pilot controlling the system. Evaluation is based on two criteria, which are the precision of reference tracking, P, and the workload, W. Workload is measured as the average number of direction changes per second in the human control input [17]. Precision is measured as the percentage of the task time spent within the desired performance boundary, the limits of which are determined as the maximum tracking errors (positive and negative) observed when the crossover model (12) operates the uncertainty-free aircraft model. The task performance index (TPX) is calculated as [17] $\text{TPX} = \frac{P^2\sqrt{W_{\min}}}{100^2\sqrt{W}}$, where $W_{\min}$ is the workload of the ideal human input. Table I shows the observed performance metrics, averaged over 16 participants. The first highlight that emerges from the data is that LSTM dramatically improves both the precision and TPX in the first two intervals. This improvement is more evident especially during the second interval, in the presence of uncertainties. In the third interval, both TPX and precision only marginally decrease for the LSTM-assisted control compared to the pilot-only case. This shows that the effect of the LSTM decreases to a sufficient degree that it does not interfere with the pilot control authority when the pilot wants to deviate from the task. This is achieved thanks to the balancing act of the modulation mechanism. As seen in Figure 4, modulation coefficient tends to be higher in the first two intervals (high LSTM effect) and decreases at the third interval (low LSTM effect). Moreover, throughout the experiments, the workload remains fairly consistent, suggesting that the assistive system does not increase the difficulty for the pilot, even when the references for the pilot and the LSTM network diverge.

APPENDIX
PROOF OF THEOREM 1

Proof: Consider the Lyapunov-Krasovskii function candidate

$$\begin{aligned} V_2 &= e_y^T(t)P_2e_y(t) + \gamma_3^{-1}\tilde{\lambda}_3^T(t)\tilde{\lambda}_3(t) \\ &+ \gamma_2^{-1}\tilde{\lambda}_2^T(t)\Lambda_2(t)\tilde{\lambda}_2(t) + \int_{-\tau}^{0}\int_{t+\nu}^{t}\dot{\tilde{\lambda}}_2^T(\xi)\dot{\tilde{\lambda}}_2(\xi)\mathrm{d}\xi\mathrm{d}\nu \\ &+ \gamma_{\phi_1}^{-1}\mathrm{Tr}\{\tilde{\Phi}_1^T(t)\tilde{\Phi}_1(t)\} + \int_{-\tau}^{0}\int_{t+\nu}^{t}\mathrm{Tr}\{\dot{\tilde{\Phi}}_1^T(\xi)\dot{\tilde{\Phi}}_1(\xi)\}\mathrm{d}\xi\mathrm{d}\nu \\ &+ \gamma_{\phi_2}^{-1}\int_{-\tau}^{0}\mathrm{Tr}\{\tilde{\Phi}_2^T(t,\eta)\tilde{\Phi}_2(t,\eta)\}\mathrm{d}\eta \\ &+ \int_{-\tau}^{0}\int_{t+\nu}^{t}\int_{-\tau}^{0}\mathrm{Tr}\{\dot{\tilde{\Phi}}_2^T(\xi,\eta)\dot{\tilde{\Phi}}_2(\xi,\eta)\}\mathrm{d}\eta\mathrm{d}\xi\mathrm{d}\nu. \end{aligned} \tag{22}$$

Following the same steps in [10], the time derivative of (22) can be calculated as

$$\begin{aligned} \dot{V}_2 \leq\ & -\lambda_{min}(Q_2)\|e_y(t)\|^2 \\ &+ \tau\left(\mu + 2\gamma_2^2\right)\|\mathrm{diag}(L_r\mathcal{G}(t-\tau))\|^2\|P_2B_p\|^2\|e_y(t)\|^2 \\ &+ \tau\left(1 + 2\gamma_{\phi_1}^2\right)\|x_p(t-\tau)\|^2\|e_y(t)\|^2\|P_2B_pL_r\|_F^2 \\ &+ \tau\left(1 + 2\gamma_{\phi_2}^2\right)\int_{-\tau}^{0}\|L_ry_h(t+\eta-\tau)\|^2\|e_y(t)\|^2\|P_2B_pL_r\|_F^2\,\mathrm{d}\eta \\ &+ 2\tau\dot{\lambda}_2^{*T}(t)\dot{\lambda}_2^*(t) + 2\tau\mathrm{Tr}\{\dot{\Phi}_1^{*T}(t)\dot{\Phi}_1^*(t)\} \\ &+ 2\tau\int_{-\tau}^{0}\mathrm{Tr}\{\dot{\Phi}_2^{*T}(t,\eta)\dot{\Phi}_2^*(t,\eta)\}\mathrm{d}\eta + 2e_y^T(t)P_2B_p\Lambda_2(t)L_ry_l(t) \\ &+ \gamma_2^{-1}\tilde{\lambda}_2^T(t)\dot{\Lambda}_2(t)\tilde{\lambda}_2(t) - 2\gamma_2^{-1}\tilde{\lambda}_2^T(t)\Lambda_2(t)\dot{\lambda}_2^*(t) \\ &- 2\gamma_3^{-1}\tilde{\lambda}_3^T(t)\dot{\lambda}_3^*(t) - 2\gamma_{\phi_1}^{-1}\mathrm{Tr}\{\dot{\Phi}_1^{*T}(t)\tilde{\Phi}_1(t)\} \\ &- 2\gamma_{\phi_2}^{-1}\int_{-\tau}^{0}\mathrm{Tr}\{\dot{\Phi}_2^{*T}(t,\eta)\tilde{\Phi}_2(t,\eta)\}\mathrm{d}\eta. \end{aligned} \tag{23}$$

Since Lemma 1 implies the boundedness of $H(t), \Lambda_2(t), \dot{H}(t)$ and $\dot{\Lambda}_2(t)$, consequently, there exist $h, \dot{h}, \beta_3, \dot{\beta}_3 \in \mathbb{R}_+$ such that $\|H(t)\| \leq h$, $\|\dot{H}(t)\| \leq \dot{h}$, $\|\Lambda_2(t)\|_F \leq \beta_3$, and $\|\dot{\Lambda}_2(t)\|_F \leq \dot{\beta}_3$ for all $t \geq t_0$. This suggests $\|\lambda_3^*(t)\| \leq \beta_3$ and $\|\dot{\lambda}_3^*(t)\| \leq \dot{\beta}_3$. Since $\hat{\lambda}_{\min_i} > 0$ for $i = 1, \ldots, m$, there exists $\beta_2 \in \mathbb{R}_+$ such that $\|\Lambda_2^{-1}(t)\|_F \leq \beta_2$. Given $\frac{\mathrm{d}\Lambda_2^{-1}}{\mathrm{d}t} = -\Lambda_2^{-1}\dot{\Lambda}_2\Lambda_2^{-1}$, there is $\dot{\beta}_2 \in \mathbb{R}_+$ such that $\|\frac{\mathrm{d}\Lambda_2^{-1}}{\mathrm{d}t}\|_F \leq \dot{\beta}_2$. Thus, for all $t \geq t_0$, $\|\lambda_2^*(t)\| \leq \beta_2$ and

$\|\dot{\lambda}_2^*(t)\| \leq \dot{\beta}_2$. Using Lemma 2 and (15) we conclude that there exist $\phi_1, \dot{\phi}_1, \phi_2, \dot{\phi}_2 \in \mathbb{R}_+$ such that $\|\Phi_1^*(t)\|_F \leq \phi_1$, $\|\dot{\Phi}_1^*(t)\|_F \leq \dot{\phi}_1$, $\|\Phi_2^*(t,\eta)\|_F \leq \phi_2$, $\|\dot{\Phi}_2^*(t,\eta)\|_F \leq \dot{\phi}_2$ for all $t \geq t_0$, $-\tau \leq \eta \leq 0$.

Using these upper bounds, and defining a constant $p \triangleq \max(\|P_2B_p\|^2, \|P_2B_pL_r\|_F^2)$, (23) can be rewritten as,

$$\begin{aligned}\dot{V}_2 \leq\ & -\lambda_{min}(Q_2)\|e_y(t)\|^2 \\ & + \tau p\left(\mu + 2\gamma_2^2\right)\|\mathrm{diag}(L_r\mathcal{G}(t-\tau))\|^2\|e_y(t)\|^2 \\ & + \tau p\left(1 + 2\gamma_{\phi_1}^2\right)\|x_p(t-\tau)\|^2\|e_y(t)\|^2 \\ & + \tau p\left(1 + 2\gamma_{\phi_2}^2\right)\int_{-\tau}^{0}\|L_r y_h(t+\eta-\tau)\|^2\|e_y(t)\|^2 \mathrm{d}\eta \\ & + 2\tau\dot{\beta}_2^2 + 2\tau\dot{\phi}_1^2 + 2\tau^2\dot{\phi}_2^2 + 2\sqrt{p}\beta_3\|e_y(t)\|\|L_r y_l(t)\| \\ & + \gamma_2^{-1}\tilde{\beta}_2^2\dot{\beta}_3 + 2\gamma_2^{-1}\tilde{\beta}_2\beta_3\dot{\beta}_2 \\ & + 2\gamma_3^{-1}\tilde{\beta}_3\dot{\beta}_3 + 2\gamma_{\phi_1}^{-1}\dot{\phi}_1\tilde{\phi}_1 + 2\gamma_{\phi_2}^{-1}\tau\dot{\phi}_2\tilde{\phi}_2, \end{aligned} \tag{24}$$

where $\tilde{\beta}_2 \triangleq \left\|\hat{\lambda}_{2max}\right\| + \beta_2$, $\tilde{\beta}_3 \triangleq \left\|\hat{\lambda}_{3max}\right\| + \beta_3$, $\tilde{\phi}_1 \triangleq \left\|\hat{\Phi}_{1max}\right\| + \phi_1$, and $\tilde{\phi}_2 \triangleq \left\|\hat{\Phi}_{2max}\right\| + \phi_2$. By defining $q \triangleq \lambda_{min}(Q_2)/p$, (24) can be rewritten as,

$$\begin{aligned}\dot{V}_2 \leq\ & p\|e_y(t)\|^2\Big(-q + \tau\Big\{\left(\mu + 2\gamma_2^2\right)\|\mathrm{diag}(L_r\mathcal{G}(t-\tau))\|^2 \\ & + \left(1 + 2\gamma_{\phi_1}^2\right)\|x_p(t-\tau)\|^2 + 2\sqrt{p}\beta_3\|e_y(t)\|\|L_r y_l(t)\| \\ & + \left(1 + 2\gamma_{\phi_2}^2\right)\int_{-\tau}^{0}\|L_r y_h(t+\eta-\tau)\|^2 \mathrm{d}\eta\Big\}\Big) \\ & + 2\tau\left(\dot{\beta}_2^2 + \dot{\phi}_1^2 + \tau\dot{\phi}_2^2\right) + \gamma_2^{-1}\tilde{\beta}_2^2\dot{\beta}_3 + 2\gamma_2^{-1}\tilde{\beta}_2\beta_3\dot{\beta}_2 \\ & + 2\gamma_3^{-1}\tilde{\beta}_3\dot{\beta}_3 + 2\gamma_{\phi_1}^{-1}\dot{\phi}_1\tilde{\phi}_1 + 2\gamma_{\phi_2}^{-1}\tau\dot{\phi}_2\tilde{\phi}_2. \end{aligned} \tag{25}$$

Lemma 1 and (14c) imply that there exist $\alpha_1 \in \mathbb{R}_+$ and $\alpha_2 \in \mathbb{R}_+$ such that $\|x_p(t)\|^2 \leq \alpha_1$ and $\|L_r y_h(t)\|^2 \leq \alpha_2$ for all $t \geq t_0$. Since $r(t)$ is bounded, and the projection operator is used in (18), $\mathcal{G}(t)$ in (14a) is bounded and there exists $\alpha_3 \in \mathbb{R}_+$ such that, for all $t \geq t_0$, $\|\mathrm{diag}(L_r\mathcal{G}(t))\|^2 \leq \alpha_3$. Since LSTM has bounded activation functions and is offline trained, for every $t \geq t_0$, there exists $\alpha_4 \in \mathbb{R}_+$ such that $\|L_r y_l(t)\| \leq \alpha_4$. Hence, (25) can be written as

$$\begin{aligned}\dot{V}_2 \leq\ & p\|e_y(t)\|^2\Big(-q + \tau\Big\{\left(\mu + 2\gamma_2^2\right)\alpha_3 + \left(1 + 2\gamma_{\phi_1}^2\right)\alpha_1 \\ & + \left(1 + 2\gamma_{\phi_2}^2\right)\tau\alpha_2\Big\}\Big) + 2\sqrt{p}\beta_3\alpha_4\|e_y(t)\| \\ & + 2\tau\left(\dot{\beta}_2^2 + \dot{\phi}_1^2 + \tau\dot{\phi}_2^2\right) + \gamma_2^{-1}\tilde{\beta}_2^2\dot{\beta}_3 + 2\gamma_2^{-1}\tilde{\beta}_2\beta_3\dot{\beta}_2 \\ & + 2\gamma_3^{-1}\tilde{\beta}_3\dot{\beta}_3 + 2\gamma_{\phi_1}^{-1}\dot{\phi}_1\tilde{\phi}_1 + 2\gamma_{\phi_2}^{-1}\tau\dot{\phi}_2\tilde{\phi}_2. \end{aligned} \tag{26}$$

Then, a sufficiently small $\tau^* \in \mathbb{R}_+$ exists that satisfies

$$\tau^*\left\{\left(\mu + 2\gamma_2^2\right)\alpha_3 + \left(1 + 2\gamma_{\phi_1}^2\right)\alpha_1 + \left(1 + 2\gamma_{\phi_2}^2\right)\tau^*\alpha_2\right\} < q. \tag{27}$$

Therefore, for any $\tau \in [0, \tau^*]$, (26) implies $\dot{V}_2 < 0$ whenever

$$\|e_y(t)\| > \frac{\sqrt{4z_2z_1 + z_3^2} + z_3}{2z_2}, \tag{28}$$

where

$$\begin{aligned} z_1 \triangleq\ & 2\tau\left(\dot{\beta}_2^2 + \dot{\phi}_1^2 + \tau\dot{\phi}_2^2\right) + \gamma_2^{-1}\tilde{\beta}_2^2\dot{\beta}_3 + 2\gamma_2^{-1}\tilde{\beta}_2\beta_3\dot{\beta}_2 \\ & + 2\gamma_3^{-1}\tilde{\beta}_3\dot{\beta}_3 + 2\gamma_{\phi_1}^{-1}\dot{\phi}_1\tilde{\phi}_1 + 2\gamma_{\phi_2}^{-1}\tau\dot{\phi}_2\tilde{\phi}_2, \\ z_2 \triangleq\ & p\Big(q - \tau\Big\{\left(\mu + 2\gamma_2^2\right)\alpha_3 + \left(1 + 2\gamma_{\phi_1}^2\right)\alpha_1 + \left(1 + 2\gamma_{\phi_2}^2\right)\tau\alpha_2\Big\}\Big), \\ z_3 \triangleq\ & 2\sqrt{p}\beta_3\alpha_4. \end{aligned} \tag{29}$$

Hence, the solution $(e_y(t), \tilde{\lambda}_2(t), \tilde{\lambda}_3(t), \tilde{\Phi}_1(t), \tilde{\Phi}_2(t,\eta))$ is bounded and converges to the compact set

$$\begin{aligned} E \triangleq \Big\{ & \Big(e_y(t), \tilde{\lambda}_2(t), \tilde{\lambda}_3(t), \tilde{\Phi}_1(t), \tilde{\Phi}_2(t,\eta)\Big): \\ & \|e_y(t)\| > \frac{\sqrt{4z_2z_1 + z_3^2} + z_3}{2z_2}, \left\|\tilde{\lambda}_2(t)\right\| \leq \tilde{\beta}_2, \\ & \left\|\tilde{\lambda}_3(t)\right\| \leq \tilde{\beta}_3, \left\|\tilde{\Phi}_1(t)\right\| \leq \tilde{\phi}_1, \left\|\tilde{\Phi}_2(t,\eta)\right\| \leq \tilde{\phi}_2\Big\}, \end{aligned} \tag{30}$$

for any $\tau \in [0, \tau^*]$. Due to the boundedness of $r(t)$, $x_m(t)$ is bounded (see (12)). In addition, since $x_p(t)$ is bounded, $e_2(t)$ is also bounded. Furthermore, $e_\Delta(t)$ is bounded since $e_y(t) = e_2(t) - e_\Delta(t)$ is bounded. This indicates that $\Delta y(t)$ is bounded, as indicated by (17). ■

REFERENCES

[1] D. A. Abbink, M. Mulder, and E. R. Boer, "Haptic shared control: Smoothly shifting control authority?" *Cogn., Technol. Work*, vol. 14, pp. 19–28, Mar. 2012.

[2] W. D. Nothwang, M. J. McCourt, R. M. Robinson, S. A. Burden, and J. W. Curtis, "The human should be part of the control loop?" in *Proc. Resilience Week (RWS)*, 2016, pp. 214–220.

[3] E. Eraslan, Y. Yildiz, and A. M. Annaswamy, "Shared control between pilots and autopilots: An illustration of a cyberphysical human system," *IEEE Control Syst. Mag.*, vol. 40, no. 6, pp. 77–97, Dec. 2020.

[4] P. Owan, J. Garbini, and S. Devasia, "Uncertainty-based arbitration of human-machine shared control," 2015, *arXiv:1511.05996*.

[5] V. Izadi, D. Saraphis, and A. H. Ghasemi, "Dynamic control authority arbitration for resolving a reverse-intent conflict in a haptic shared control paradigm," *IFAC-PapersOnLine*, vol. 55, no. 37, pp. 512–517, 2022.

[6] S. Xu, W. Tan, A. V. Efremov, L. Sun, and X. Qu, "Review of control models for human pilot behavior," *Annu. Rev. Control*, vol. 44, pp. 274–291, Oct. 2017.

[7] M. Y. Uzun, E. Inanc, and Y. Yildiz, "Enhancing human operator performance with long short-term memory networks in adaptively controlled systems," *IEEE Control Syst. Lett.*, vol. 7, pp. 3507–3512, 2023.

[8] A. Habboush and Y. Yildiz, "An adaptive pilot model with reaction time-delay," in *Proc. IEEE 61st Conf. Decision Control (CDC)*, 2022, pp. 38–43.

[9] S. S. Tohidi, Y. Yildiz, and I. Kolmanovsky, "Adaptive control allocation for constrained systems," *Automatica*, vol. 121, Nov. 2020, Art. no. 109161.

[10] A. Habboush and Y. Yildiz, "An adaptive pilot model with reaction time-delay," 2022, *arXiv:2208.13303*.

[11] A. Habboush and Y. Yildiz, "An adaptive human pilot model for adaptively controlled systems," *IEEE Control Syst. Lett.*, vol. 6, pp. 1964–1969, 2021.

[12] C.-T. Chen, *Linear System Theory and Design*, 3rd ed. New York, NY, USA: Oxford Univ. Press, Inc., 1998.

[13] A. Graves, *Long Short-Term Memory*. Berlin, Germany: Springer, 2012, pp. 37–45.

[14] L. Sun, C. C. de Visser, Q. P. Chu, and W. Falkena, "Hybrid sensor-based backstepping control approach with its application to fault-tolerant flight control," *J. Guid., Control, Dyn.*, vol. 37, no. 1, pp. 59–71, 2014.

[15] B. L. Stevens, F. L. Lewis, and E. N. Johnson, *Aircraft Control and Simulation: Dynamics, Controls Design, and Autonomous Systems*. Hoboken, NJ, USA: Wiley, 2015.

[16] Y. Yildiz, A. M. Annaswamy, D. Yanakiev, and I. Kolmanovsky, "Spark-ignition-engine idle speed control: An adaptive control approach," *IEEE Trans. Control Sys. Tech.*, vol. 19, no. 5, pp. 990–1002, Sep. 2011.

[17] P. Perfect, M. Jump, and M. D. White, "Handling qualities requirements for future personal aerial vehicles," *J. Guid., Control, Dyn.*, vol. 38, no. 12, pp. 2386–2398, 2015.